EXPRESSION OF ENDOPLASMIC RETICULUM OXIDOREDUCTASES (EROS) AND THEIR ROLE IN THE GI TRACT

GRAEME WATSON

CHAPTER 4

EXPRESSION AND PURIFICATION OF ERO1B

4.1 Introduction

The ERO1-Lβ gene was discovered following a database search using the ERO1-Lα gene as an input sequence (Pagani *et al.*, 2000). The ERO1-Lβ gene has a ~75% similarity with and ~65% identity to ERO1-Lα. One of the main conserved features between Ero1α and Ero1β is the redox-active CXXCXXC motif, whilst a key difference is the number of glycosylation sites present on Ero1β compared to Ero1α. Ero1β has been localised to the ER, and is known to co-localise with PDI and calnexin (Pagani *et al.*, 2000). Ero1β shows a particularly high expression in stomach and pancreas (Dias-Gunasekara *et al.*, 2005). Although the exact role of Ero1β is unclear, it may be required for secretion of specialised proteins such as insulin (Zito *et al.*, 2010). Unpublished data from the Benham group (Dias-Gunasekara and Benham, 2006-2007) suggested that Ero1β may also be present in tissues from patients with Barrett's oesophagus or adenocarcinoma, the role of which is unknown, but may be important in the development of new biomarkers for this disease.

Previously, data in Chapter 3 showed a considerable difference in Ero1α expression between OE21 and OE33 using Western blot analysis. In this chapter, basal levels of Ero1β expression, putative alternate splice conformations and its expression in response to known ER stressors were examined in oesophageal cancer cells. RT-PCR was used and primers were designed specifically to amplify each putative alternate splice variant. In order to characterise the biochemical function of Ero1β, a HIS-GST fusion protein was purified, and this in turn was used to generate monoclonal antibody supernatants that were tested for reactivity to Ero1β (this data is shown in Chapter 5).

4.2 Results

4.2.1 Ero1β expression, detection of alternate splice forms

In silico examination of the ERO1β gene shows that it has been annotated with three alternate splice variants (Figure 4.1). However, whether these are expressed in mammalian tissue, in addition to the 16 exon full length sequence, is not known.

To differentiate between Ero1β splice variants, expression was determined using RT-PCR with unique primers for each of the three variants.

Using data from ensembl, primers were designed that were specific to each of the three variants that are 4, 7 and 16 exons in length (Table 4.1A). The shorter splice variants share similar sequences to the 16 exon wildtype. The forward primers 1F and 2F were cross reactive with Ero1β-16/7 and Ero1β-16/4 respectively. The reverse primers 3R and 4R were also cross reactive with Ero1β-16/7 and Ero1β-16/4 respectively. Both the reverse primers 5R and 6R were unique to Ero1β-4 and 7 respectively. By choosing appropriate combinations of each of these primers, it was possible to differentiate between splice variants, by generating PCR products that could be easily differentiated from one another on agarose gel (Table 4.1B).

The primers were checked using NCBI primer BLAST to verify that they were not cross-reactive against any other sequence in the database. In initial PCR validation experiments, the primers were tested against the Ero1β-myc construct. Figure 4.2 shows a PCR using different primers against Ero1β-myc construct DNA. As expected, actin primers gave no PCR product (Figure 4.2, lane 1) whereas the full length 16-exon Ero1β-myc construct gave a 982 bp PCR product, as predicted (lane 4). No signal was seen either for Ero1β-7 or 4 (Figure 4.2, lane 2-3).

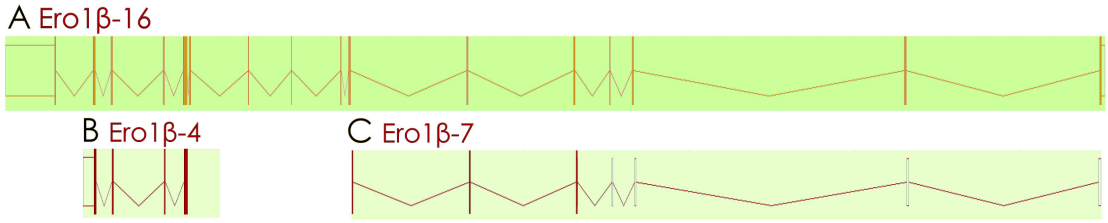

Figure 4.1: Schematic showing the three putative splice variants of Ero1β

Schematic showing exon arrangements, represented by vertical bars, of the three putative splice variants of Ero1β, containing 16, 4 or 7 exons.

A: Full-length Ero1β-16 (16 exons). B: Ero1β-4 (4 exons). C: Ero1β-7 (7 exons). Note, both Ero1β-4 and Ero1β-7 are mapped against Ero1β-16. Figure modified from data generated by ensembl.org (Gene ID: ENST00000354619)

Table 4.1 Ero1β alternate splice sequence primers

A

Simple Name	Forward	Reverse	Exon Specificity
1F	TCCGGTTGGAATAAAAGCTG	-	16 and 7
2F	TGTGGAAACCAAGGGAGAAG	-	16 and 4
3R	-	GCTCTGGGTTCAGCAATAGG	16 and 7
4R	-	ATTTCCTGTCGGGTGAGTTG	16 and 4
5R	-	CTTTTTCCCCAAGGAAGCAT	Unique for 4
6F	GGGCCAGAAAAGAGGTGATT	-	Unique for 7

B

Splice Variant	Primer Combination	Forward	Reverse	Product Size
E001 (16 Exons)	1F and 4R	TCCGGTTGGAATAAAAGCTG	ATTTCCTGTCGGGTGAGTTG	**982**
E002 (7 Exons)	6F and 3R	GGGCCAGAAAAGAGGTGATT	GCTCTGGGTTCAGCAATAGG	**551**
E003 (4 Exons)	2F and 5R	TGTGGAAACCAAGGGAGAAG	CTTTTTCCCCAAGGAAGCAT	**1090**

A: This table shows the adopted names and sequences for each of the Ero1β primers sequences. The final column gives the specificity to each of the Ero1β splice variants, 16, 7 and 4.

B: This table shows the primer combinations that were used to determine specific Ero1β splice variant expression, primer sequences and calculated product size on gel.

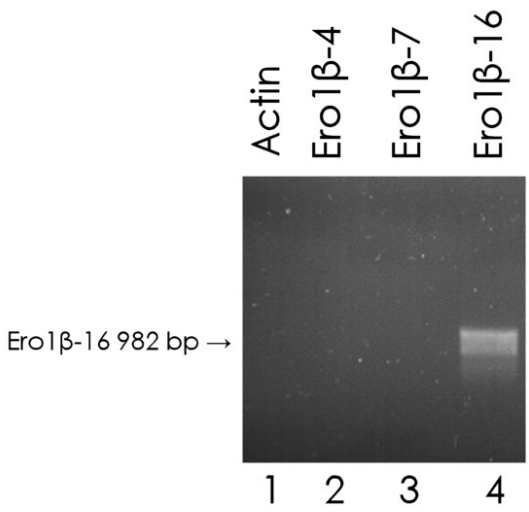

Figure 4.2: RT-PCR Validation of Ero1β primers

PCR for actin and Ero1β 4, 7 and 16 exon variants, Ero1β-myc DNA was used as a template in all samples.

Although one primer in each pair that was used to probe for either the 4-exon or 7-exon variant was cross reactive with the wildtype, the one unique primer in each set ensured specificity. Thus this experiment shows that the primers specific for alternative Ero1β splice forms do not cross-prime with wt Ero1β.

Next, the Ero1β primers were compared at two different melting temperatures on the PCR block (Figure 4.3) because the melting temperatures of actin and BiP (51.8-59.1^{o}C "standard") differed slightly compared to the melting temperatures calculated for the Ero1β variant primers (59.5-60.49 ^{o}C "alternate"). Each of the two temperatures was compared (standard versus alternate), using RNA from HeLa cells treated for 6 hours with tunicamycin. The data showed broadly comparable results, that similar levels of PCR product were obtained for actin and BiP at both temperatures (lanes 1, 7 and 2, 8 respectively). Although the PCR reaction worked for the positive control cDNA (lanes 6, 12), Ero1β expression was not upregulated in HeLa following 6 hour tunicamycin treatment (Figure 4.3, lanes1-5, 7-11). Expression of the putative alternative Ero1β-4/7 exon transcripts was not seen. Following this experiment, it was decided to anneal subsequent PCRs at 58 °C.

The lack of upregulation of Ero1β in response to tunicamycin treatment was unexpected and investigated further, by comparing the expression of Ero1β in response to tunicamycin treatment in HeLa, OE21 and OE33 cell lines.

Figure 4.4A shows the results of an RT-PCR analysis of 6 hour tunicamycin treated HeLa, OE21 and OE33 cells. RNA samples from each of these cell lines were subjected to PCR with primers for Ero1β-16, and actin respectively.

Basal expression of Ero1β-16 was not seen in HeLa, OE21 or OE33 pre-treatment (Figure 4.4 lanes 1-3). This did not change following 6 hour tunicamycin treatment, which was unexpected (Figure 4.4 lanes 4-7).

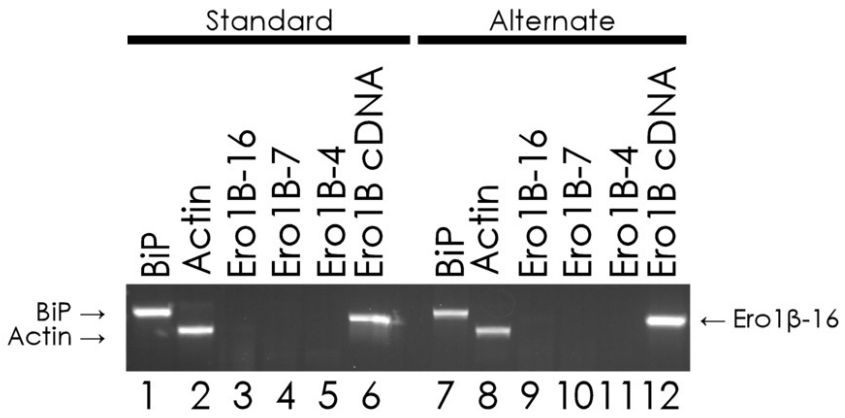

Figure 4.3: Expression of Ero1β variants after tunicamycin treatment

RT-PCR showing the expression of BiP, actin and Ero1β following a 6 hour tunicamycin treatment of HeLa cells using standard PCR cycle (lanes 1-5) or an alternative PCR cycle, (lanes 7-11). Lanes 6 and 12 are the Ero1β-myc 16 exon cDNA construct positive control. Both the standard and alternate temperature conditions amplified BiP, actin and control Ero1β-16.

A

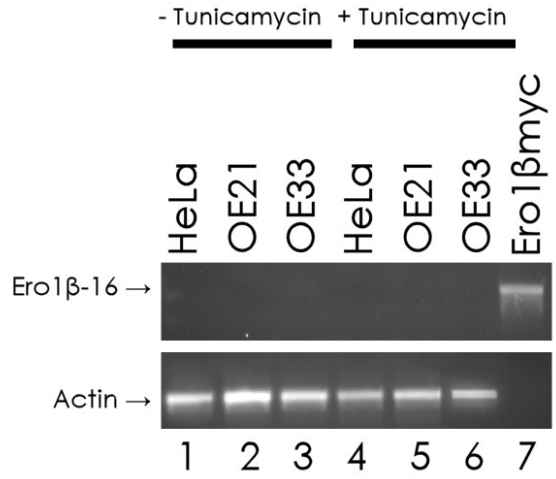

Figure 4.4: Expression of Ero1β mRNA +/- tunicamycin and protein in oesophageal cell lines

A: HeLa OE21 and OE33 were subjected to a 6 hour tunicamycin treatment (upper panel, lanes 4-6), and were compared to untreated samples (upper panel, lanes 1-3). An RT-PCR was performed with each sample, assessing Ero1β-16 expression. Actin was used as a positive control for the PCR (lower panel). Ero1β-myc cDNA was used as a positive control for the Ero1β-16 primers.

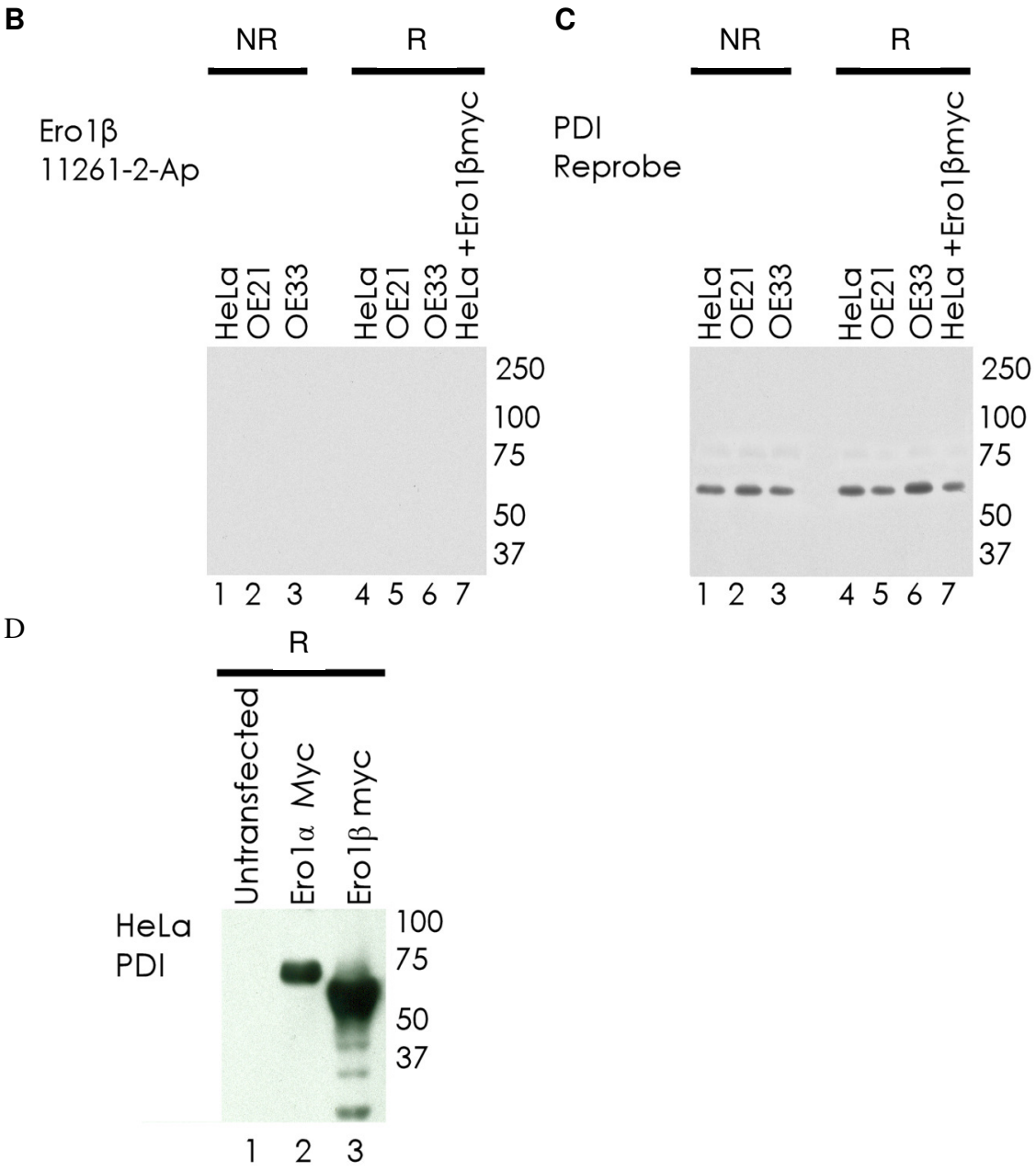

Figure 4.4 (Cont): Expression of Ero1β mRNA +/- tunicamycin and protein in oesophageal cell lines

B: SDS-PAGE of protein lysates following 6 hour tunicamycin treatment, run under non-reducing (lanes 1-3) and reducing (lanes 4-6) conditions. The polyclonal antibody 11261-2-AP (Proteintech) gave a negative signal for Ero1β. C. A PDI reprobe of the membrane showed in B verifying the loading and transfer of the lysates shown in B. D: A Western blot for Myc, which verified the Ero1β-myc transfectant alongside the Ero1α-myc transfectant.

The Ero1β-myc positive control verified that the Ero1β PCR had worked (Figure 4.4A lane 7) and the actin positive control confirmed that equal amounts of RNA/DNA were amplified and loaded. To further investigate putative Ero1β expression in HeLa, OE21 and OE33 cells, the commercial antibody 11261-2-AP (Proteintech) was tested against these cell lines and a lysate of HeLa cells transfected with Ero1β-myc. Samples were run under reducing and non-reducing conditions in an attempt to determine the oxidation state of Ero1β in these cell types (Figure 4.4B, PDI reprobe 4.4C). Although according to the manufacturer, 11261-2-AP is positive for Ero1β in pancreatic tissue (unpublished), the antibody did not give a positive signal on Western blot. The cell lines themselves were negative, as was the transfected sample. The Ero1β transfectant is shown further in Chapter 5, and can be identified by either the myc or HIS tag on the protein.

Having been unable to induce Ero1β expression by tunicamycin treatment, a range of other ER stress stimuli were used. Expression of Ero1β variant sequences Ero1β-4 and Ero1β-7 was examined by RT-PCR in HeLa, following a number of 6 hour treatments in serum-free media with tunicamycin, thapsigargin or A21387. Figure 4.5 shows data from this experiment. No signal was seen from the Ero1β 4 or 7 primers. The unavailability of a positive control construct means that it remains possible, albeit highly unlikely, that alternative transcripts are expressed at a low level. Finally, BiP expression was characteristically upregulated in response to the UPR induced either by tunicamycin, thapsigargin or A21387 (lanes 3-6 compared to the untreated controls lanes 1 and 2). The upregulation of BiP demonstrated that the drug treatments were effective in HeLa cells.

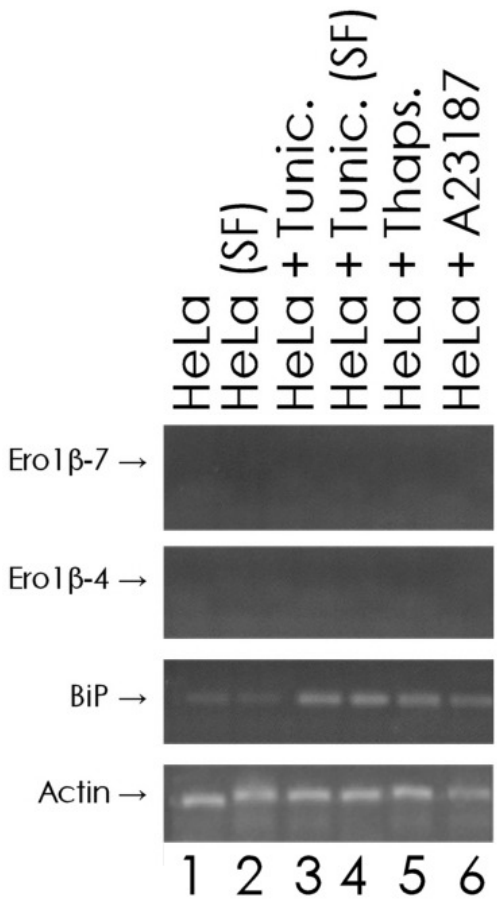

Figure 4.5: RT-PCR comparing expression of Ero1β-16, 7 and 4 with BiP and actin following ER stress treatments

HeLa cells were treated with a number of exogenous ER stressors (serum-free media, tunicamycin, thapsigargin and A23187). The samples were processed using RT-PCR and expression of Ero1β-16, Ero1β -7 and 4 was assessed in treated or untreated cells. Actin levels were used as a positive control for the sample and to verify loading.

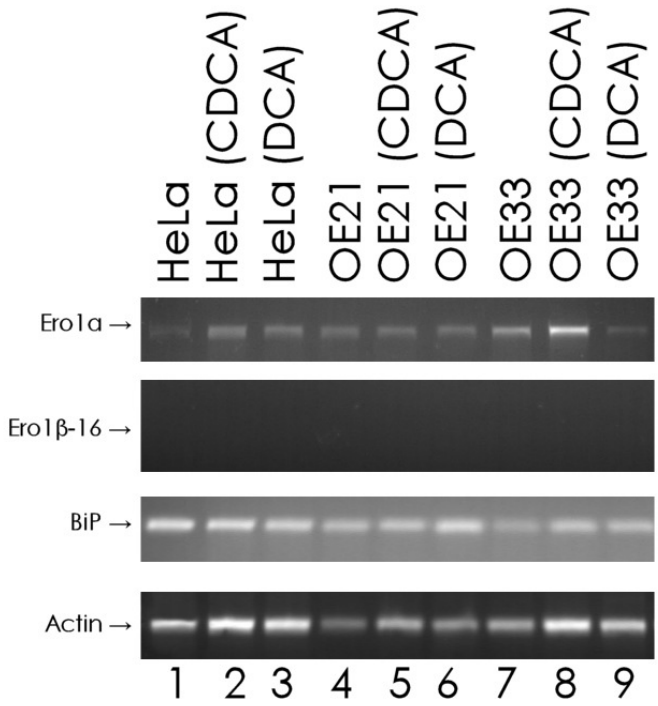

Figure 4.6: RT-PCR comparing expression of Ero1β-16, 7 and 4 with BiP and actin following bile acid treatments

HeLa, OE21 and OE33 cells were treated for 6 hours using chenodeoxycholic acid (CDCA) and deoxycholic acid (DCA). In each treatment, an untreated control is shown. The samples were processed to determine Ero1α, Ero1β-16, BiP and actin expression. Samples were verified for loading with actin.

Having found that Ero1β was undetectable using conditions that upregulated BiP, alternative stressors such as bile acids were tested to find their influence on the expression of Ero1β. As a final experiment in the series, Ero1β expression was assessed, comparing untreated HeLa, OE21 and OE33 with 6 hour treatments of chenodeoxycholic acid (CDCA) and deoxycholic acid (DCA). The expression of Ero1β was compared to Ero1α, BiP and actin in the same PCR series. Figure 4.6 shows results from this experiment. Ero1α was present in each sample, lowest in HeLa, and somewhat higher in OE33 (consistent with the results obtained by Western blot in Chapter 3). It is possible that the 6 hour treatment of CDCA in OE33 resulted in an increase of Ero1α expression, though the corresponding actin also showed a similarly higher signal than elsewhere in the series, suggesting the elevated Ero1α result in lane 8 may be artifactual. This, alongside blot data shown in Chapter 3 suggests that Ero1α expression is not influenced by these bile acids, at least under the conditions used in this thesis. No expression of Ero1β was evident in untreated or treated cells, either with known ER stressors, or with bile acid treatment. Given these results, it was clear that good antibodies against Ero1β were required to better understand its function and relationship with Ero1α.

4.3 Protein purification

Given the need for better Ero1β antibodies, and the requirement for recombinant protein to understand the biochemistry of Ero1β, a system for expressing Ero1β and its substrates was developed. PDI and TRX are both model substrates for Ero function (Sevier *et al*., 2007), although had not been used in oxygen electrode recordings with Ero1β. These were both purified using protocols that are outlined in Chapter 2 and described in detail below.

4.3.1 Purification of PDI and TRX

PDI and TRX proteins were expressed in BL21 *E.coli* after induction by IPTG. Bacterial pellets were lysed and purified using nickel agarose purification, and buffer exchanged using PD10 columns. Proteins were concentrated using vivaspin columns. Figures 4.7-4.8 show SDS-PAGE gels of the fractions derived from the principle purification steps in the production of PDI. Figure 4.7, lane 1 shows "Total Lysate"; this was a sample derived from the unfiltered, unpurified bacterial culture pellet and contained many proteins. The "Soluble Fraction" and "Insoluble Fraction" (Lanes 2 and 3 respectively) were derived following centrifugal clarification of the lysed pellet, and were also impure. The "Ni-NTA unbound" and associated wash fractions (lanes 4-6) were fractions collected from these steps in the protocol, and contained the majority of impurities that did not bind to the Ni-NTA column. The "Elution" fraction was from the eluate following Ni-NTA incubation (lane 7). Lane 9 shows the final PDI sample derived from the purification. This was further purified by a vivaspin column and buffer exchanged using a PD10 column. PDI was clearly visible around the 66kDa marker, but there were a number of impurities, especially at the 29 kDa marker.

Evidently, the end products of the first purification run did not produce a sufficiently pure sample of PDI for use in biochemical analyses.

Figure 4.8 shows another purification of PDI, again showing sample fractions from the principle purification steps, as outlined in Figure 4.7. For this purification, the starting material was expanded from a number of cultures. The final elution fraction in lane 7 had only one minor contaminant lying around 50 kDa. Following vivaspin and buffer exchange, the final PDI sample shown in lane 8 was deemed suitable for use in assays.

Following successful production of PDI, the next protein needed was thioredoxin (TRX). This was to be used as an electron acceptor in oxygen electrode recordings with Ero1β (method outlined in Chapter 2, section 2.7.4), using a method published by the Bulleid group for Ero1α (Baker *et al*., 2008). Production of TRX was similar to PDI as outlined above (see Chapter 2 for protocol). Figure 4.9 shows fractions collected from the principle purification steps of TRX from BL21 bacterial cells. Here, lane 1 shows uninduced BL21cell lysate. Lane 2 shows a sample taken following 1 hour of induction, and lane 3 shows a sample from bacterial lysate at the end of the culture period. The insoluble and soluble fractions of the clarified lysate are shown in lanes 4-5. As for PDI, Ni-NTA was used to purify TRX, and these steps are shown in lanes 6-8. Lane 9 shows TRX, which migrated close to the 14 kDa marker as expected. Note the number of other impurities present in this final sample, around 97, 66 and 29 kDa. As this TRX was too impure for use, previously purified stocks from the Bulleid group were used in biochemical assays.

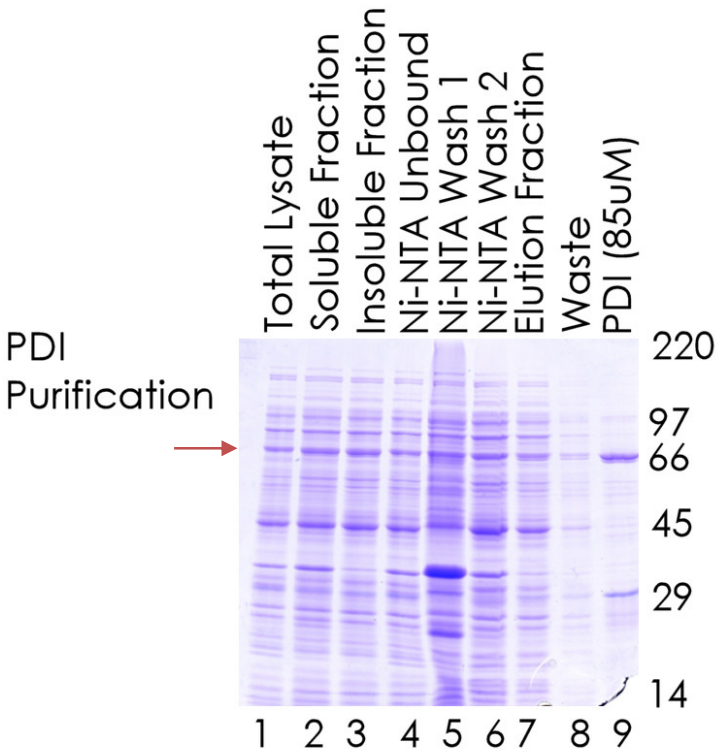

Figure 4.7: Purification of PDI in BL21 *E. coli*

PDI was expressed in BL21 *E.coli*. Bacterial pellets were lysed and purified using nickel agarose purification, and buffer exchanged and concentrated using PD10 and vivaspin columns. This Coomassie gel shows the main purification fractions from the initial PDI purification. The band at around 66kDa is PDI, and is highlighted with an arrow.

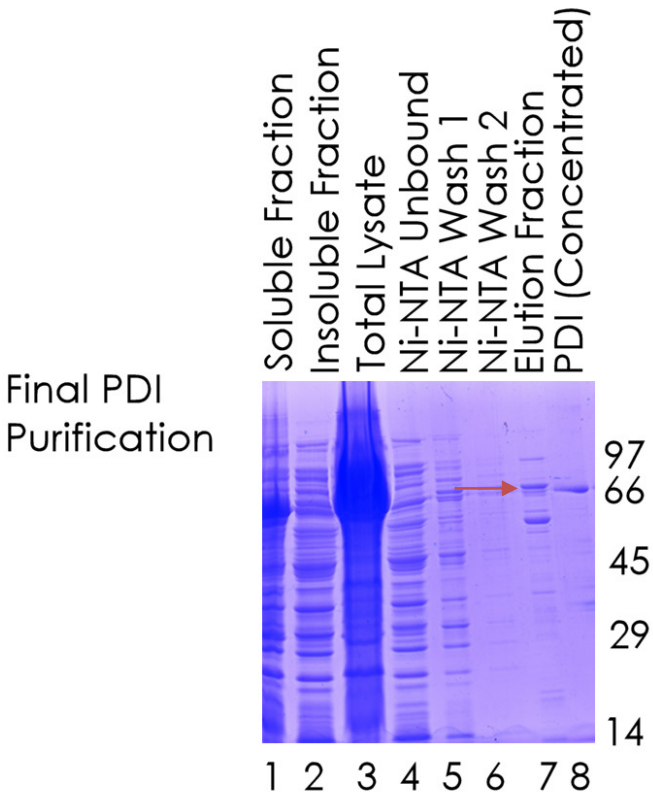

Figure 4.8: Final purification of PDI in BL21 cells

PDI was expressed in BL21 *E.coli*. Bacterial pellets from a number of cultures were lysed and purified using nickel agarose purification, before being buffer exchanged and concentrated using PD10 and vivaspin columns. This Coomassie stained gel shows the main fractions in the final PDI purification, and the final concentrated sample of PDI (lane 8). The band at around 66 kDa (lane 9) is PDI, and is labelled with an arrow.

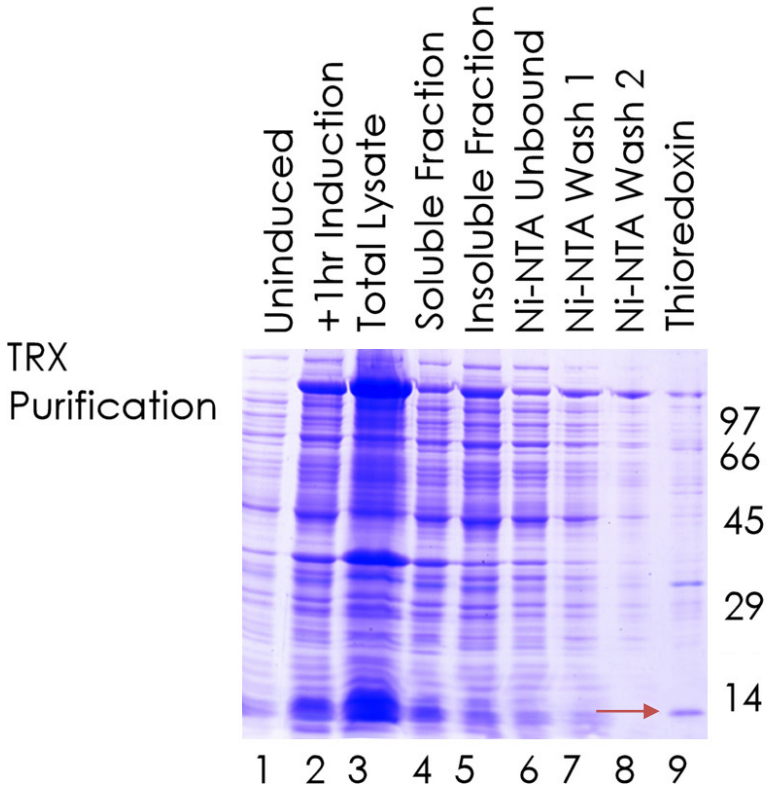

Figure 4.9: Purification of thioredoxin

TRX was expressed in BL21 *E.coli*. Bacterial pellets were lysed and purified using nickel agarose purification, before being buffer exchanged and concentrated. This Coomassie gel shows unsuccessful purification steps in the production of thioredoxin. Note the number of impurities that were present. TRX runs at 12 kDa (see arrow).

4.3.2 Purification of Ero1β

Following the successful purification of PDI, work was begun to purify Ero1β, according to the protocol established by the Bulleid group for Ero1α (Baker *et al*., 2008). All details of the initial and (later) optimised purification protocol for Ero1β are outlined in Chapter 2.

4.3.2.1 Initial purification and functional tests of Ero1β

Ero1β-HIS-GST (PGEX4T-3 vector) was expressed in origami cells that have mutations in both the thioredoxin reductase and glutathione reductase genes, which enhances disulphide bond formation in the cytoplasm. The protocol outlined here involves production of a dual tagged protein, Ero1β-HIS-GST. Predicted running sizes of the Ero1β recombinant proteins are shown in Figure 4.10. The GST tag can be used to purify the recombinant protein using glutathione sepharose beads, and the tag can then be cleaved by thrombin. A 5ml starter culture was used to inoculate 500 ml of sterile LB containing antibiotics and cultured for 6 hours at 37.5 °C.

At the end of this growth period, the culture was induced with 500 μM IPTG and 10mM FAD for 24 hours at 16 °C to induce Ero1β-HIS-GST protein expression.

The following day, the culture was centrifuged, pelleted, resuspended in a PBS wash buffer, and snap-frozen. The frozen pellet was lysed, and underwent a snap-freeze-thaw cycle. The lysate was clarified, and incubated with Ni-NTA beads. That which had bound to the nickel agarose column was then washed and eluted, buffer exchanged via PD10, and thrombin cleaved for 3 hours at 4 °C. This was then gravity filtered in a chromatography column.

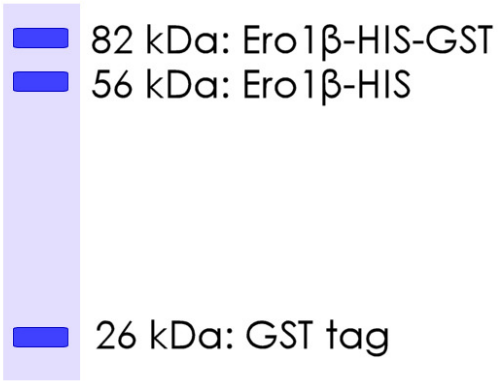

Figure 4.10: Predicted running sizes of Ero1β recombinant proteins

This figure outlines the predicted running sizes Ero1β recombinant products based on the molecular weights of Ero1β, the HIS and GST tags.

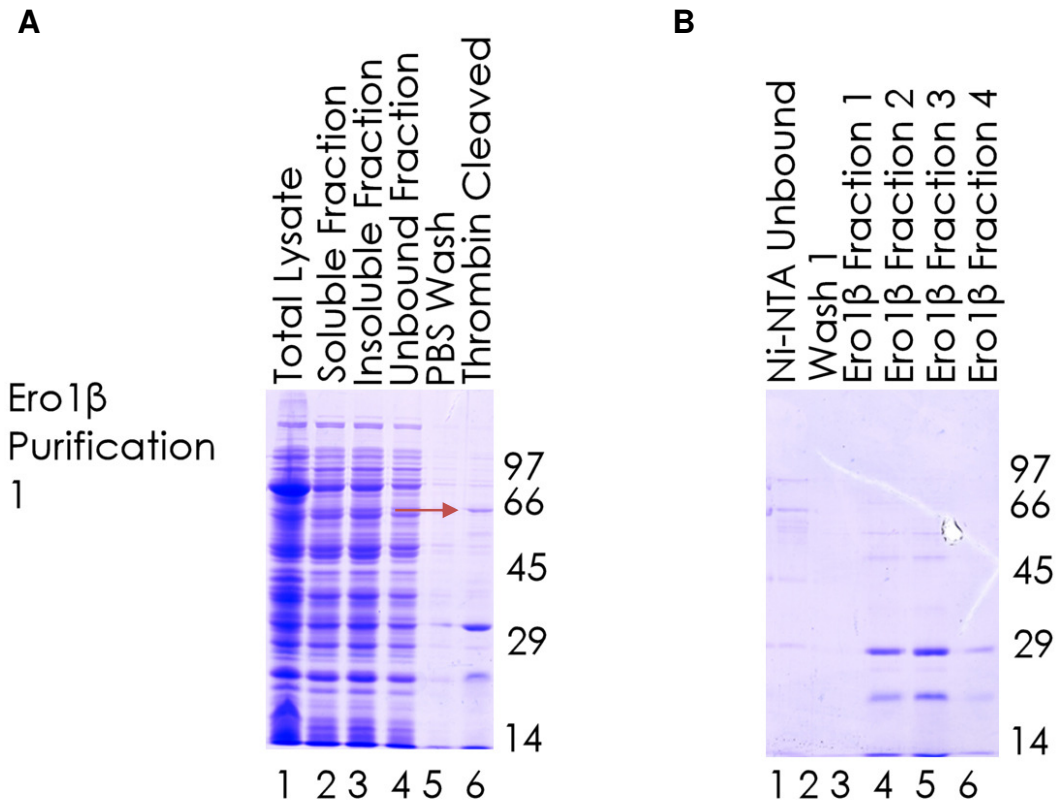

Figure 4.11: Initial purification steps in the production of Ero1β-HIS

Ero1β-HIS-GST (PGEX4T-3 vector) was expressed in origami cells. The culture lysate was clarified, incubated with Ni-NTA beads, washed, eluted, buffer exchanged and thrombin cleaved for 3 hours at 4 °C. These Coomassie gels show fractions derived from the purification steps. A: Lanes 1-5 show samples taken from each step in the purification process. Lane 6 shows the final, thrombin-cleaved Ero1β sample. Ero1β is indicated with an arrow. B: Subsequent preparations contained very little Ero1β, but the same contaminants seen in A, around and below 30 kDa.

The flow though contained Ero1β-HIS, while the GST tag remained attached to the beads. Figure 4.11 shows fractions collected during the principle parts of the protocol. Figure 4.11A shows total unfiltered cell lysate, the soluble and insoluble fragments following lysis and clearing (lanes 1-3). These samples contained many contaminating proteins. The unbound fraction (lane 4) shows that the majority of these impurities were unbound in the Ni-NTA column.

Thrombin was used to cleave the GST tag from the construct, leaving only the HIS tag behind. The final thrombin cleaved sample showed an Ero1β-HIS band at around the 66 kDa marker (lane 7). However, there were a number of impurities, especially around 29 kDa and below. This rendered the sample unsuitable for use in biochemical assays. Figure 4.11B shows elution samples from four other Ero1β preparations (lanes 3-6). These showed similar impurities as Figure 4.11A. This was initially believed to be due to either instability of the Ero1β product produced, or as a result of non-specific thrombin cleavage.

To solve this issue, both Ero1β stability over time and the thrombin cleavage timepoint were optimised. (Figures 4.12 and 4.13). In figure 4.12, Ero1β stability over time at both 4 °C and room temperature is shown. For this, samples of Ero1β were incubated at the indicated time points, with the results shown on Coomassie gel. It was clear that for each timepoint, the end products on gel were similar. This suggested that the fusion protein was in fact stable from 1-24 hours at 4 °C or 24 °C, and ruled out thermal instability as a cause of the impurities seen in the later stages of the Ero1β preparation. Following this, the time at which Ero1β-HIS-GST was incubated with thrombin to cleave the GST tag was varied, and compared both at the standard 4 °C, and room temperature (Figure 4.13).

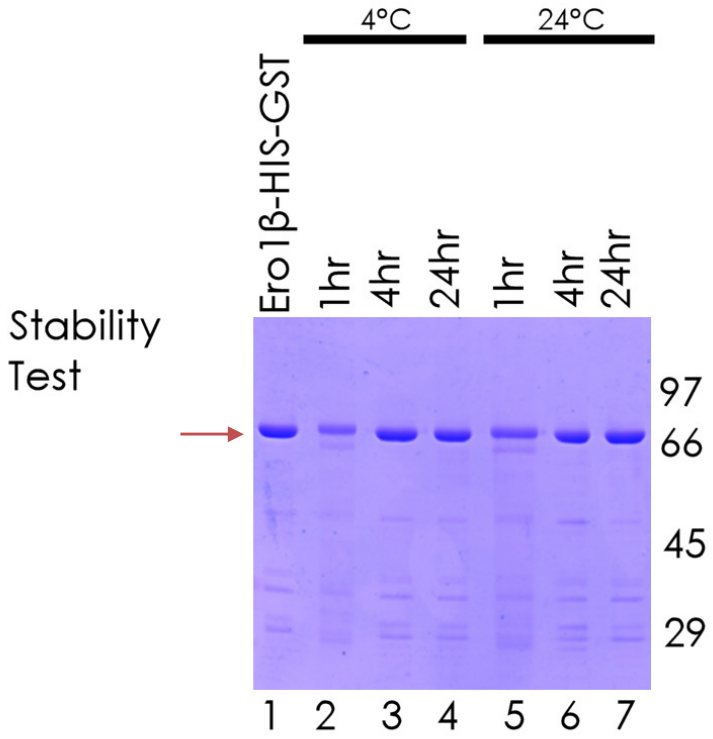

Figure 4.12: Coomassie gel showing Ero1β-HIS-GST stability

This gel shows the stability of Ero1β-HIS-GST, indicated with an arrow, over 1, 4 and 24 hour periods, both at 4 °C and 24 °C. The number and character of fragments seen on gel in each lane was comparable between lanes, showing that Ero1β (major band around 66kDa) is in fact stable over the time points and temperatures used.

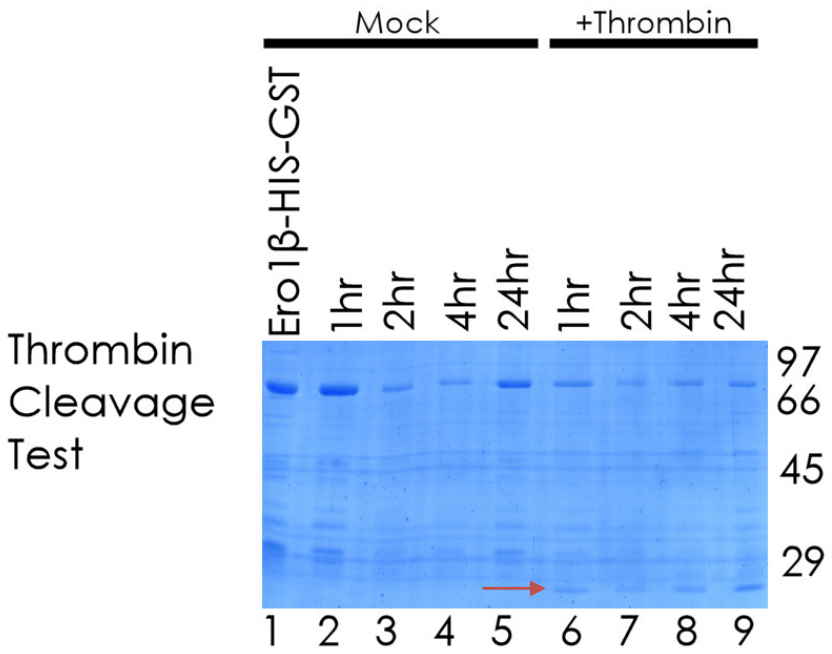

Figure 4.13: Thrombin cleavage stability test at 4 °C

This coomassie gel shows Ero1β after incubation +/- thrombin (100 units ml^{-1}) for1, 2, 4 and 24 hour time periods. Despite some variance in loading in lanes 1 and 2, Ero1β remained stable up to 24 hours at 4 °C. In the thrombin cleavage series (lanes 6-9), the GST tag is seen below 29 kDa, lane 9 (highlighted with an arrow). No non-specific cleavage ran over these timepoints. This indicated that the thrombin cleavage part of the protocol was unlikely to be responsible for the impure Ero1β seen in the earlier purifications.

Following incubation with thrombin, from 1-24 hours, the end products on gel were similar. Ero1β remained stable at 4 °C up to 24 hours in the presence of thrombin (100 $unitsml^{-1}$). Figure 4.13 lane 1 shows Ero1β-HIS-GST from frozen stock, and remained stable at 4 °C from 1-24 hours (lanes 2-5) and at 4 °C in the presence of thrombin (100 $unitsml^{-1}$) from 1-24 hours. Lanes 6-9 show that the GST tag was cleaved from Ero1β-HIS-GST fusion protein, and was visible below the 29 kDa marker as a single band. This showed that the thrombin incubation time period was unlikely to be responsible for the non-specific fragmentation seen during purification.

Following these optimisation experiments, a number of Ero1β purifications were carried out with slight modifications (not shown). A final purification was performed, that resulted in the production of pure Ero1β-HIS.

4.3.2.2 Final purification and testing of Ero1β

Following the optimisations outlined in the previous section, the Ero1β purification protocol was improved and a pure sample was produced. The final procedure for this was described in Chapter 2, and outlined as a flow diagram in Figure 4.14. The key differences in the optimised protocol are that there were two rounds of Ni-NTA HIS purification, and the GST tag was thrombin cleaved whilst the fusion protein was bound to the GST beads. Figure 4.15 shows fractions collected during the principle purification steps, up to the Ni-NTA elution. The Ni-NTA elutions shown in lanes 7 and 8 contain Ero1β-HIS-GST, and a number of other impurities (Stage 4, day one in Figure 4.14). The Ero1β-HIS-GST band in lanes 7 and 8 is highlighted by an arrow in the Figure 4.15.

Figure 4.16A shows the purification steps from Day 1, stage 5, as detailed in Figure 4.14. Note that after GST cleavage, two principle bands were seen in lane 4; the upper band was the higher molecular weight fusion protein Ero1β-HIS-GST. The lower band

was Ero1β-HIS. Having gone through a second round of Ni-NTA purification (steps shown in lanes 5-7) the final sample (Figure 4.16B, lane 8) showed only Ero1β-HIS. The majority of impurities seen in early purifications, and the upper Ero1β-HIS-GST band were no longer present.

This protocol was repeated a number of times to generate sufficient Ero1β-HIS for biochemical assays and for use as an immunogen for monoclonal antibody production. Figure 4.17 shows a direct comparison between Ero1β samples obtained using the initial (lane 1) and final protocol (lane 2). The number of impurities seen using the initial protocol was greatly decreased when the GST was cleaved whilst the fusion protein was attached to the GST beads, and underwent a second round of Ni-NTA purification.

Once Ero1β-HIS could be reproducibly purified, it was suitable for use in biochemical assays with PDI and TRX. Figure 4.18 shows a thioredoxin assay, which assessed the oxidation state of TRX (Sevier *et al.*, 2007). TRX was modified with the thiol alkylating agent, AMS, to increase the mass of TRX so that gel migration was slower. Should the oxidation state of TRX change, it would be trapped by the AMS. Figure 4.18A shows that TRX underwent no change in oxidation state following the addition of Ero1β, compared to no Ero1β at all. If Ero1β was to function as Ero1α (Sevier *et al.*, 2007, Baker *et al*., 2008), one would have expected that TRX would change from its reduced form seen in lane 2, to a lower oxidised form. One would have expected a midpoint for two distinct TRX bands to exist, in both the reduced and oxidised state. For Ero1α, this occured over 10 minutes (600 seconds, lane 6). Here, Ero1β-HIS as purified was incapable of oxidising TRX. Figure 4.18B shows a silver stained gel, that shows Ero1β over the same timepoints. One would have expected a change from the reduced to oxidised state, but again it remained stable in the reduced state. This data

suggested that Ero1β-HIS as purified was either inactive or could not utilise TRX as redox partner.

Nevertheless, the Ero1β-HIS was used in an oxygen electrode assay with PDI in the presence of GSH. Although gel assays suggested that purified Ero1β-HIS was inactive with TRX, when it is studied in a reaction of PDI with GSH, oxygen consumption was comparable to Ero1α over a similar timescale, as shown by Baker *et al*., 2008. Figure 4.19 shows that 292 $nmolml^{-1}$ of oxygen is consumed over 44 minutes in the reaction, in Baker *et al*. 180 $nmolml^{-1}$ of oxygen is consumed over 50 minutes in the reaction of Ero1α with PDI. This result suggested that Ero1β-HIS was active against its physiological partner, PDI, but not against TRX

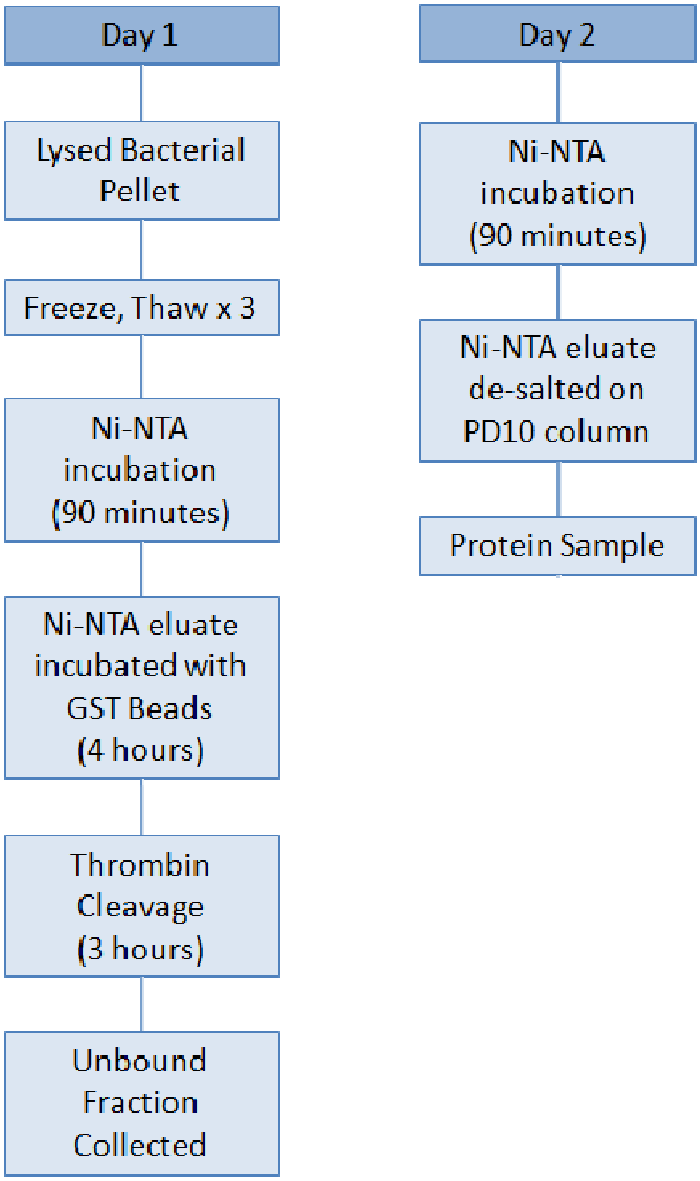

Figure 4.14: Outline of the optimised Ero1β purification protocol

This schematic shows a simple overview of the steps necessary to purify Ero1β, without non-specific thrombin cleavage. The key feature of this protocol is the double Ni-NTA incubation on day 1 and the beginning of day 2.

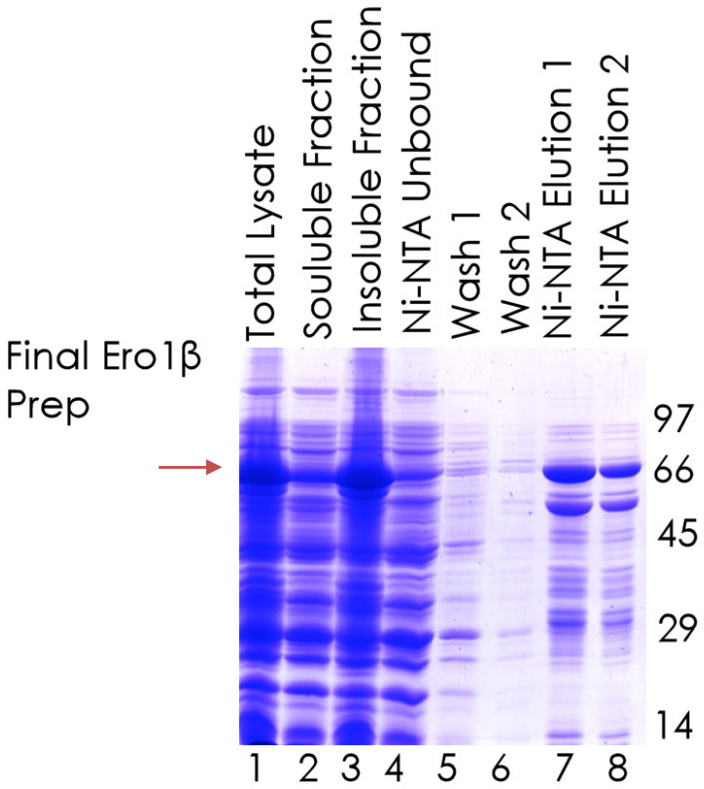

Figure 4.15: Optimised purification of Ero1β-HIS

Ero1β-HIS-GST (PGEX4T-3 vector) was expressed in origami cells. The culture lysate was clarified, incubated with Ni-NTA beads, washed, eluted, buffer exchanged and thrombin cleaved for 3 hours at 4 °C. Following this, the sample underwent a further Ni-NTA incubation cycle. This Coomassie gel shows the principle purification fractions obtained during the final production of Ero1β-HIS, up to the nickel agarose incubation steps and elutions (Day 2, as outline in Figure 4.14). Note the very strong Ero1β band at 66 kDa (indicated by an arrow).

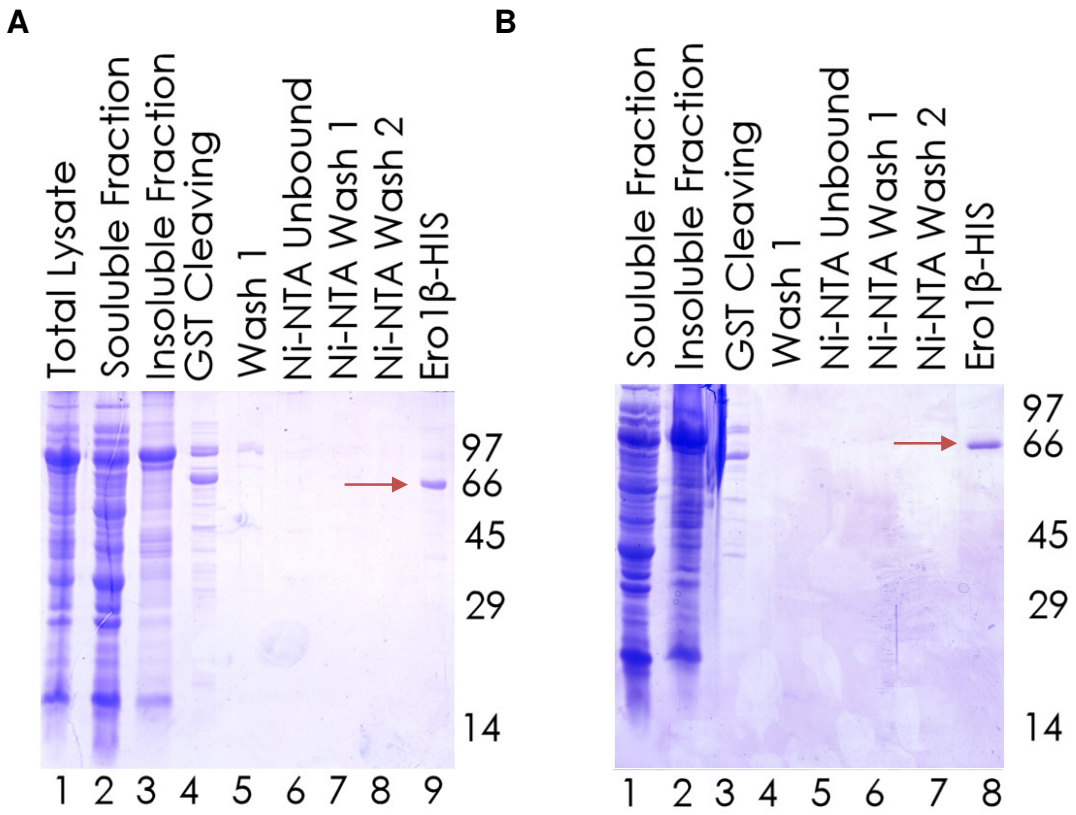

Figure 4.16: Final purification of Ero1β, showing GST removal with Thrombin

A: Coomassie gel showing the initial three purification steps (lanes 1-3), and the removal of the GST tag with thrombin, following on from Figure 4.15.

Note the principle upper and lower bands in lane 4 were Ero1β-HIS-GST and Ero1β-HIS respectively. The final sample seen in lane 8 was Ero1β-HIS (indicated by an arrow). B: Duplicate experiment to show the reproducibility of the Ero1β purification protocol. Lane 3 shows the presence of Ero1β-HIS-GST (lane 3, upper band) and Ero1β-HIS (lane 3, lower band). Lane 8 shows Ero1β-HIS, which had the GST tag removed, and had no contaminating protein present in the sample.

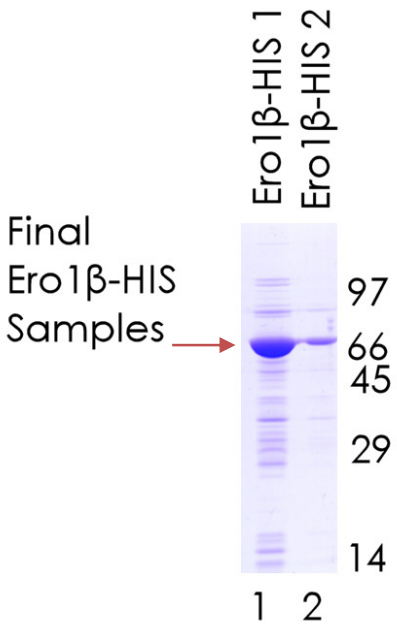

Figure 4.17: Comparison of Ero1β-HIS generated by the two protocols

This gel shows Ero1β-HIS (arrow) after thrombin cleavage using the initial protocol, concentrated using the vivaspin column (lane 1). Lane 2 is as lane 1, but from the second protocol.

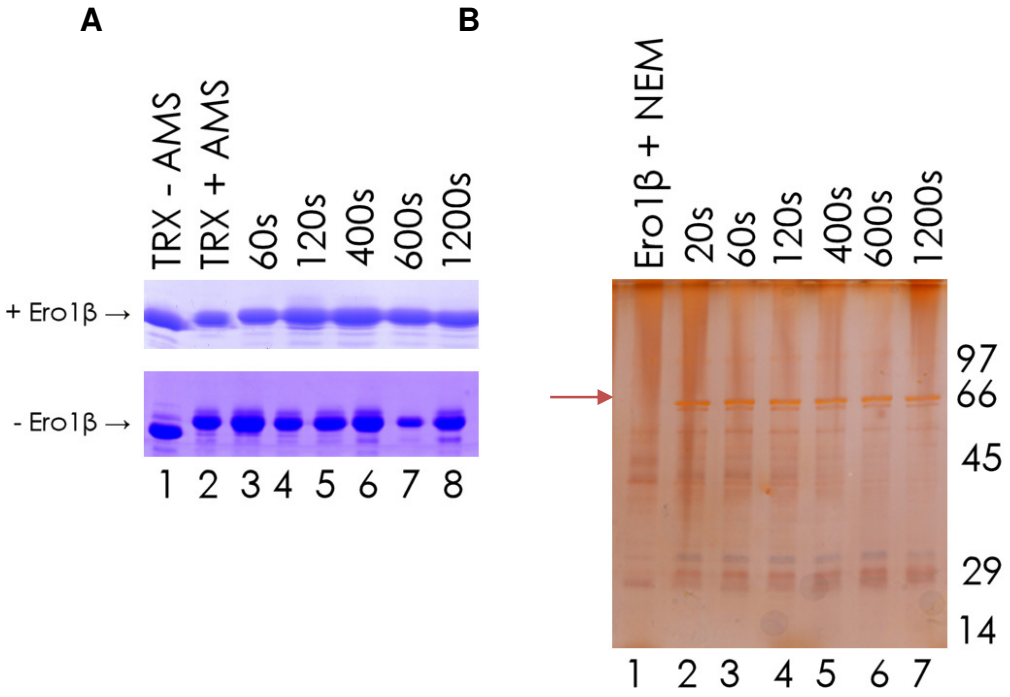

Figure 4.18: Assay of TRX and Ero1β-HIS

A: Coomassie stained gel of the reaction between TRX and Ero1β-HIS, over timepoints from 60-1200 seconds, and analysed by reducing SDS-PAGE. B: Silver stained gel of the reaction of Ero1β with reduced TRX. Oxidation state was quenched with NEM. Timepoints are shown from 20 – 1200 seconds.

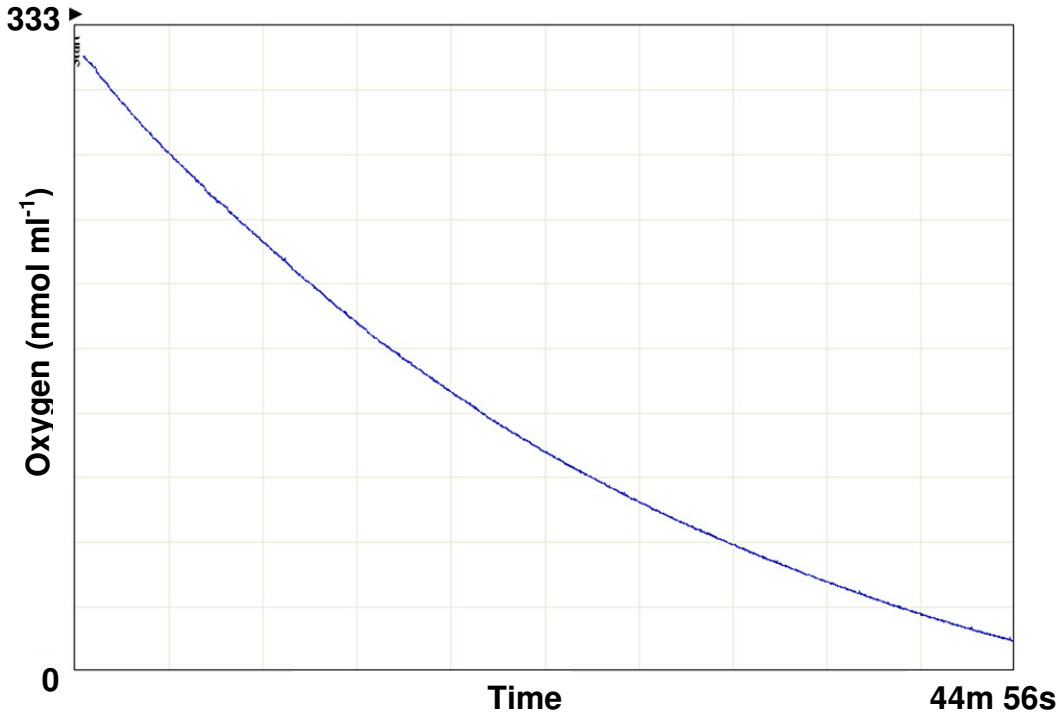

Figure 4.19: Oxygen electrode recording of the reaction between Ero1β-HIS and reduced PDI in the presence of GSH

This shows the consumption of oxygen over a period of 44 minutes, in the reaction of Ero1β with PDI in the presence of glutathione. Over a period of 44 minutes, 292 $nmolml^{-1}$ of oxygen was consumed, suggesting that there was some Ero1β activity, based on similar data produced by Ero1α (Baker *et al*., 2008).

4.4 Discussion

The alternate splice sequences of Ero1β were investigated in HeLa, OE21 and OE33, under standard ER stress conditions, and following bile acid treatment. In order to better examine the expression and role of Ero1β, it was purified as a fusion protein, and tested for function with thioredoxin and PDI.

The gene database Ensembl suggests two additional splice sequences for Ero1β, which contain either 4 or 7 exons, in contrast to the full length16 exons. Using RT-PCR and primers designed specific for each alternate sequence, the primer sets were checked against the full length construct (Figure 4.2). Neither Ero1β-4 nor Ero1β 7 could be seen in cells, or following ER stress treatments with tunicamycin or with bile acids (Figure 4.3, Figure 4.4). Ero1α protein expression was shown in Chapter 3 using Western blot, and here, Ero1α mRNA expression was profiled using RT-PCR. Either using Western blot (Chapter 3), or RT-PCR, Ero1α expression was consistently higher in OE33 than in OE21 (Figure 4.6).

High innate BiP expression was seen in OE33 cells in Figure 4.3, suggesting that this cell line shows some adaptation for a stressful environment. High BiP expression has been seen previously in the chief cells of the stomach, and adenocarcinoma cells often become more like cell types found below the level of the oesophago-gastric junction (Dias-Gunasekara *et al.*, 2005). Increased BiP expression (as shown by mRNA changes) seen in advancing stages of primary resected human oesophageal adenocarcinomas may be indicative of ongoing ER stress, either by hypoxia, glucose starvation or the effect of bile acids (Langer *et al.*, 2008). Following on from the bile acid treatments described in Chapter 3, and analysed by Western blot, Ero1α and Ero1β expression at the mRNA level was explored using RT-PCR. Data in chapter 3 showed that Ero1α was expressed in the HeLa, OE21 and OE33 cell lines. RT-PCR data

(Figure 4.6) shows that the expression of Ero1α at the mRNA level is highest in OE33 cells, and that this is not influenced by CDCA or DCA treatment. Ero1β was not expressed in HeLa, OE21 or OE33 at the level of mRNA, nor does this change following CDCA or DCA treatment.

It was surprising to find that tunicamycin did not upregulate Ero1β expression (Figure 4.4). However, other experiments in the laboratory suggest that Ero1β may not be induced as easily as some other UPR target genes (Lemin and Benham, unpublished, 2010)

In the second half of this chapter, it was shown that PDI and Ero1β could be expressed and purified. The published purification method for Ero1α (Baker *et al*., 2008) was not suitable for the purification of Ero1β, without modification (Figure 4.14). When purified, Ero1β was stable both at 4 °C and 24 °C for up to 24 hours, without showing signs of degradation (Figure 4.12 and 4.13). It was not capable of oxidising reduced TRX in the manner seen both in Ero1p and Ero1α (Figure 4.18) (Sevier *et al.*, 2007, Baker *et al*., 2008). Although this may suggest that purified Ero1β-HIS was inactive, in the reaction of PDI with GSH (Figure 4.19), oxygen consumption was comparable to that published for Ero1α over a similar timescale (Baker *et al*., 2008). These data suggested that PDI but not TRX is a suitable substrate for Ero1β *in vitro*.